ISSN 1330-3651 (Print), ISSN 1848-6339 (Online)
https://doi.org/10.17559/TV-20230206000327
Original scientific paper

# Prediction of the Vortex Evolution and Influence Analysis of Rough Bed in a Hydraulic Jump with the Omega-Liutex Method

Cong Trieu TRAN*, Cong Ty TRINH

**Abstract:** The dissipation of energy downstream of hydropower projects is a significant issue. The hydraulic jump is exciting and widely applied in practice to dissipate energy. Many hydraulic jump characteristics have been studied, such as length of jump *Lj* and sequent flow depth $y_2$. However, understanding the evolution of the vortex structure in the hydraulic jump shows a significant challenge. This study uses the RNG *k-ε* turbulence model to simulate hydraulic jumps on the rough bed. The Omega-Liutex method is compared with *Q*-criterion for capturing vortex structure in the hydraulic jump. The formation, development, and shedding of the vortex structure at the rough bed in the hydraulic jumper are analyzed. The vortex forms and rapidly reduces strength on the rough bed, resulting in fast dissipation of energy. At the rough block rows 2nd and 3rd, the vortex forms a vortex rope that moves downstream and then breaks. The vortex-shedding region represents a significant energy attenuation of the flow. Therefore, the rough bed dissipates kinetic energy well. Adding reliability to the vortex determined by the Liutex method, the vorticity transport equation is used to compare the vorticity distribution with the Liutex distribution. The results show a further comprehension of the hydraulic jump phenomenon and its energy dissipation.

**Keywords:** flow-3D; hydraulic Jump; omega-liutex method; vortex breakdown

## 1 INTRODUCTION

The past decade has witnessed excellent computational fluid dynamics (CFD) development through the rapid development of computer technology. Many studies have presented a new methodological approach based on CFD, in which the problem of determining the spin in hydraulic jumps is increasingly exciting and studied [1]. Therefore, the model and calculation method have been significantly improved.

The hydraulic jump is a simple and effective method of dissipating the excess kinetic energy of the flow [2]. A hydraulic jump is carried out to reduce the damage to downstream structures. It has been applied in engineering to dissipate the energy of high-velocity flow in irrigation-hydroelectric projects, such as spillways and water gates. The velocities of downstream flow are often substantial, and excess kinetic energy will destroy the foundation of the downstream construction if not dissipated in time. The energy flow is converted into turbulent flow [3], causing a strong vortex in the flow and an increase in the flow depth simultaneously. Over the decades, various rough bed types have been studied to control hydraulic jumps and dissipate energy [4, 5]. Through experiments, many authors have focused on studying characteristics such as decreased energy, velocity distribution, jump length, sequent depth, and shear stress [3, 5]. The rough bed results in a 60% reduction in jump length compared to a smooth bed [3]. The rapid energy dissipation due to roughness caused much turbulence in the flow. However, those researchers focused on exploring parameters such as length and depth. The properties of flow turbulence in hydraulic jumps, such as vortex evolution in 3D flow, have not been thoroughly predicted.

Researchers have attempted to clarify vortex in turbulence flow, and many identification methods of the vortex have been introduced. In engineering, the widely used vortex identification method in turbulent flow is *Q*-criterion [6]. However, the *Q*-criterion challenges choosing a suitable threshold value. Recently, in an attempt to overcome these limitations, Gao and Liu [7]. introduced the Omega method; then, in 2019, Liu [8, 9] continued to introduce the Liutex/Rortex method. The vortex structure in turbulence flow can be more accurately described by the Omega method when Omega has a value of 0.52 [10]. Liutex provides a variety of vortex detection and visualization methods, such as Liutex iso-surface, Liutex vectors, and Liutex cores. However, the Liutex iso-surface for vortex detection is still influenced by the choice of a threshold value. Although the Liutex iso-surface is not very sensitive to the threshold value, it is not too difficult to choose a suitable value [11]. Due to these shortcomings, the Omega-Liutex method was proposed by Dong et al. [12], by merging the advantages of the Omega method and Liutex methods. Consequently, with the threshold value of 0.52, the vortex structure can be determined rigorously and uniquely by the Omega-Liutex method.

Accurate identification of the vortex structure and its evolution is essential for studying swirl flow. The Omega-Liutex method has apparent advantages for the precise and quantitative breakdown of vortex characteristics in turbulence flow [13-15]. Therefore, this study focuses on investigating the vortex structure evolution in the turbulent flow of hydraulic jumps based on the geometry, parameters, and experimental results published by Bejestan and Neisi [3]. In the present work, the hydraulic jumps are simulated using the RNG k-ε turbulence model and VOF method. The vortex strength and the iso-surface of the Omega - Liutex method are used to investigate vortex behavior and energy dissipation of a hydraulic jump on the rough bed. The Liutex distribution and the vorticity in the hydraulic jumps were compared accurately and quantitatively. The rough bed influences the turbulent structure and demonstrates the roughness of bed's energy dissipation mechanism. The periodical vortex rope behaviors and the vortex breakdown phenomena on the rough bed are further revealed.

## 2 MATHEMATICAL METHOD

When a hydraulic jump occurs, the flow in the channel is turbulent, so the general equations in the turbulent flow must be considered in the simulation.

### 2.1 Governing Equations

The turbulence flow can be described by the continuity equation, the momentum equation, and a transport equation called the governing equation.

$$\frac{\partial \rho}{\partial t}+\frac{\partial(\rho u_i)}{\partial x_j}=0 \tag{1}$$

$$\frac{\partial(\rho u_i)}{\partial t}+\frac{\partial(\rho u_i u_j)}{\partial x_j}=\frac{\partial \rho}{\partial x_i}+\frac{\partial}{\partial x_j}\left[(\mu+\mu_t)\left(\frac{\partial u_i}{\partial x_j}+\frac{\partial u_j}{\partial x_i}\right)\right] \tag{2}$$

where $\rho$ - the density; $u_i$, $u_j$ - the absolute velocity components; $\mu$ - the kinematic viscosity; $\mu_t$ - the turbulence viscosity.

### 2.2 Vortex Identification Methods

*a) Liutex method*

The critical feature of the Liutex method is that it is possible to use the iso-surface of Liutex, the vector field, and the Liutex streamlines to describe the vortex structure, vortex direction, vortex magnitude, and vortex core line, as published in [9, 14-16]. According to those publications, the vector and magnitude of Liutex ($R$) are defined as follows:

$$\vec{R}=R\vec{r} \tag{3}$$

$$R=\begin{cases}2(\beta-\alpha), & \alpha^2-\beta^2<0\\ 0, & \alpha^2-\beta^2>0\end{cases} \tag{4}$$

$$\alpha=\frac{1}{2}\sqrt{\left(\frac{\partial v}{\partial y}-\frac{\partial u}{\partial x}\right)^2+\left(\frac{\partial v}{\partial x}+\frac{\partial u}{\partial y}\right)^2} \tag{5}$$

$$\beta=\frac{1}{2}\left(\frac{\partial v}{\partial x}-\frac{\partial u}{\partial y}\right)^2 \tag{6}$$

$$\nabla v=\begin{bmatrix}\frac{\partial u}{\partial x} & \frac{\partial u}{\partial x} & 0\\ \frac{\partial v}{\partial x} & \frac{\partial v}{\partial y} & 0\\ \frac{\partial w}{\partial x} & \frac{\partial w}{\partial y} & \frac{\partial w}{\partial z}\end{bmatrix} \tag{7}$$

*b) $\Omega_R$ (Omega-Liutex) method*

Unlike most traditional vortex identifiers, the $\Omega_R$ in the $\Omega_R$ method is dimensionless. The $\Omega_R$ varies between 0-1 and represents the fluid deformation. Liu et al. demonstrate that in a fluid flow, a vortex is formed when $\Omega_R = 0.52$, and $\Omega_R$ is defined like this: (8), i.e. [12].

$$\Omega_R=\frac{\beta^2}{\alpha^2+\beta^2+\varepsilon} \tag{8}$$

where $\alpha$ and $\beta$ are defined by Eqs. (5), (6), respectively, $\varepsilon = b_R(\beta^2-\alpha^2)_{\max}$ with $b_R = 0.001$ is used in this work.

### 2.3 Numerical Setup

This work used the experimental data published by Bejestan and Neisi [3]. The dimensions of the channel bed and roughness elements used in the experiments are kept intact in the model. In the experiment, Bejestan and Neisi used rough beds, which are lozenge rough element shapes (rough blocks) with a height and width of 16 mm. The crest of the rough block is at the same level as the up and downstream bed. The distance between the edges of the blocks is 22.6 mm, and the spacing of the first and second rows of blocks is 32 mm. Fig. 1 and Tab. 1 show the numerical model and boundary conditions also used to simulate the hydraulic jumps on the rough bed.

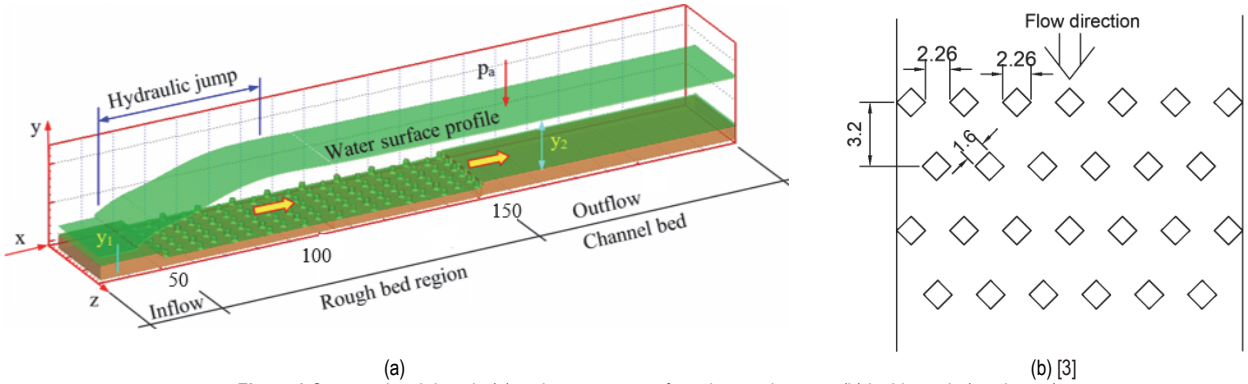


(a) (b) [3]

**Figure 1** Computational domain (a) and arrangement of roughness elements; (b) in this study (centimeter)

**Table 1** Experimental result of Bejestan and Neisi [3]

| $q$ / m$^3$/sm | $v_1$ / m/s | $y_1$ / m | $Fr_1$ | $Re_1$ | $y_2$ / m | $L_j$ / m |
|---|---|---|---|---|---|---|
| 0.0531 | 2.657 | 0.02 | 6.00 | 52616 | 0.124 | 0.64 |

where $q$ is the unit discharge; $v_1$ is the velocity of inflow; $y_1$ is inflow depth, $Fr_1$ is inflow Froude number; $Re_1$ is the Reynolds number; $y_2$ is the sequent flow depth; $L_j$ is the length of jump.

The Flow-3D commercial computational fluid dynamics software was used to solve the three-dimensional unsteady flow in a hydraulic jump on the rough bed. Although there are many turbulent models like $k$-$\varepsilon$, $k$-$\omega$,

LES in Flow-3D, the Renormalization Group RNG $k$-$\varepsilon$ model is widely used for simulations of a hydraulic jump [5, 17]. This model has an improved turbulent shear stress transport, a more stable algorithm, and an improved simulation performance for the flow in narrow spaces [1]. Therefore, the turbulent model (RNG $k$-$\varepsilon$) is used in this work. The water surface is calculated by the VOF method for this simulation.

The hydraulic jump regime is complicated, requiring a high-quality mesh rather than downstream. Therefore, in this model, we divided it into two blocks, as shown in Fig. 2a. Block 1 is the whole model; Block 2 is the rough bed and hydraulic jump zone with a finer mesh size. The computational domain is a structured rectangular hexahedral mesh. The selected mesh size should be a divisor of the geometrical dimensions of the work, denoted in 3 dimensions as $\Delta x$, $\Delta y$, and $\Delta z$, respectively, in Tab. 2. In this work, two mesh sizes are selected (grid 1 is coarse mesh and grid 2 is fine mesh) to perform the numerical simulation. This mesh size has been used in many studies and is proven suitable in simulation results [18]. The wall function method is used in the Flow-3D model. The dimensionless mesh thickness $y^+$ in the 1st layer of the boundary layer is equal to 73, which meets the requirement of the wall function method ($30 < y^+ < 300$). Therefore, the results of the RNG $k$-$\varepsilon$ turbulence model are acceptable. The simulation mesh is illustrated in Fig. 2a.

The flow in the calculation domain is placed in the cartesian coordinate system consisting of 6 sides. The inlet is assigned the flow velocity $v_1$ and the water level at the beginning of channel $y_1$, where the flow is determined in a fast-flowing state with Froude number, $Fr_1$ = 6.0. The outlet (downstream) is set the environmental pressure ($P$) with the downstream flow depth $y_2$. The channel bottom is assigned as a rigid wall. The highest boundary on the $Z$ axis is assigned atmospheric pressure ($P$). The two-sides $Y$-direction are assigned a symmetry boundary ($S$). The arrangement of boundary conditions in the simulation model is shown in Fig. 2b. For details of boundary condition values, see Tab. 1.

**Table 2** Simulated grid size parameters

| Grid | Block 1<br>$\Delta x = \Delta y = \Delta z$ / mm | Block 2<br>$\Delta x = \Delta y = \Delta z$ / mm |
|---|---|---|
| Grid 1 | 5.0 | 2.5 |
| Grid 2 | 4.0 | 2.0 |

**Table 3** Deviations of sequent depth ratio ($y_2/y_1$) for the refined grid 1 (G1) and coarse grid 2 (G2) model compared to experiment

| | $y_2/y_1$<br>Experiment [3]<br>/ m | $y_2/y_1$<br>This paper<br>/ m | Error<br>/ % |
|---|---|---|---|
| G1 | 6.20 | 6.39 | 3.06 |
| G2 | 6.20 | 6.27 | 1.13 |

This simulation found a close agreement with the experimental value obtained by Bejestan and Neisi [3] in the sequent depth ratio ($y_2/y_1$) relative error of about 3.06 % for grid 1(coarse grid) and about 1.05 % for grid 2 (refined grid). For this work, the refined grid 2 (G2) is selected for simulation.

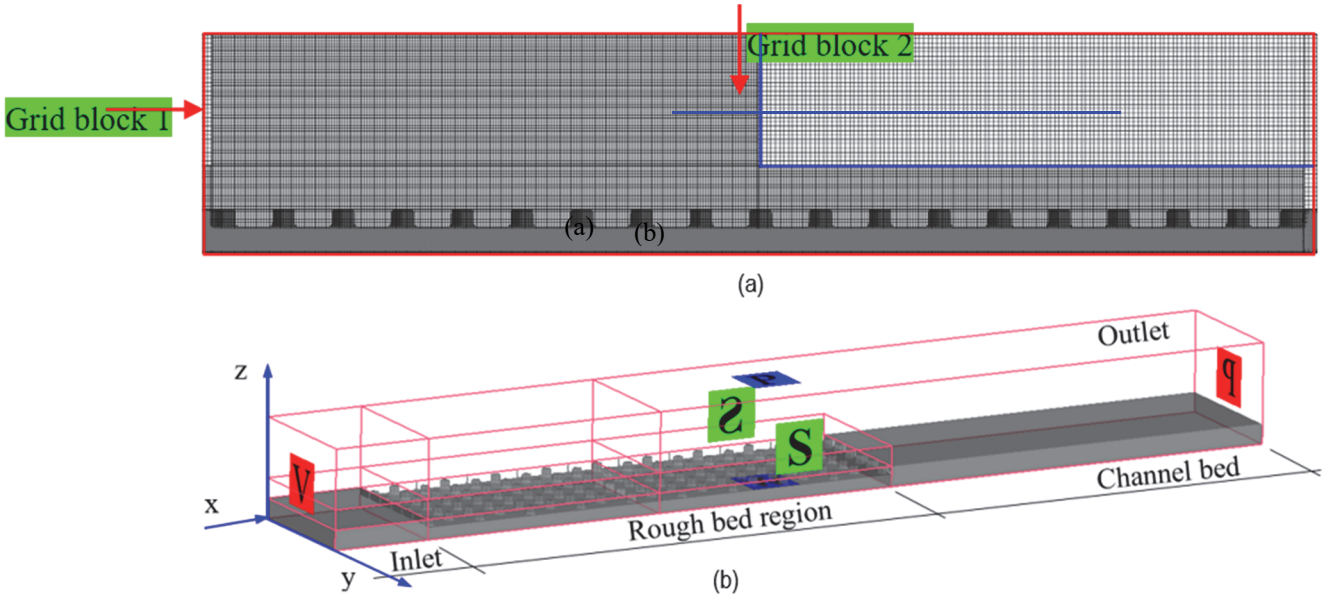


**Figure 2** Grid (a) and boundary conditions (b)

## 3 RESULTS AND ANALYSES

### 3.1 Validation of CFD Results

For validation of the results from the numerical modeling, the water surface of the hydraulic jump obtained from the simulation is compared with the experimental by Bejestan and Neisi [3]. In this study, the sequent depth ratio ($y_2/y_1$) was used to check the agreement of the numerical model and experiment data (see Tab. 4).

**Table 4** Deviations of sequent depth ratio ($y_2/y_1$) and ratio of hydraulic jump length to sequent depth ($L_j/y_2$) for the numerical result compared to experiment

| | $y_1/y_2$ | $L_j/y_2$ | $Fr_1$ |
|---|---|---|---|
| This paper | 6.27 | 4.21 | 6.0 |
| Experiment [3] | 6.20 | 4.15 | 6.0 |
| Deviations / % | 1.13 | 1.44 | 0.0 |

This simulation result found a close agreement with the experimental value obtained by Bejestan and Neisi [3] in the sequent depth ratio ($y_2/y_1$) relative error of about 1.13

% and the ratio of hydraulic jump length to sequent depth ($L_j/y_2$) relative error of about 1.44 %.

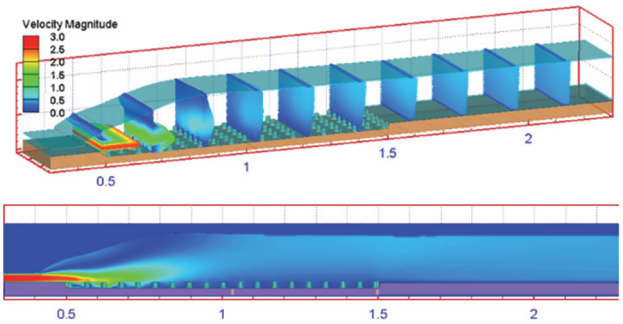


**Figure 3** Simulation results: (a) 3D velocity profiles; (b) 2D velocity field

Fig. 3 shows the instantaneous velocity values. The numerical results obtained for velocity, inflow depth ($y_1$), Froude number, sequent flow depth ($y_2$), and length of jump considered are like experimental results [3]. With the agreement between the experimental and numerical results, the overall accuracy of the simulation is acceptable.

### 3.2 Vortex Structure

Along the channel, the flow is divided into three regions: region 1 is the upstream hydraulic jump beginning area; region 2 is the hydraulic jump; region 3 is the zone of stable flow after the hydraulic jump (Fig. 4). Fig. 4 compares the evolution of the vortex structure identified by the $Q$-criterion and $\Omega_R$ method. The figure showed a graphic similarity between the results of the $Q$-criterion and the $\Omega_R$ method in capturing the vortex structure. $Q$-criterion has broad filed values (0 to 107900), so it is difficult to accurately capture vortex structures; choosing a threshold value is challenging for researchers. With different values of threshold, the vortex structure was also different, as shown in Figs. 4a, b, and c. Under the influence of a rough bed, the vortex breakdown occurring at the beginning of a rough bed (region 2) is visualized by the $Q$-criterion even when a small threshold value is selected. This phenomenon does not fully reflect the properties of the hydraulic jump because, in this area, the hydraulic jump takes place firmly, as shown by the rapid increase in water depth. In addition, because of the boundary layer, a non-vortex zone appeared at the inlet region.

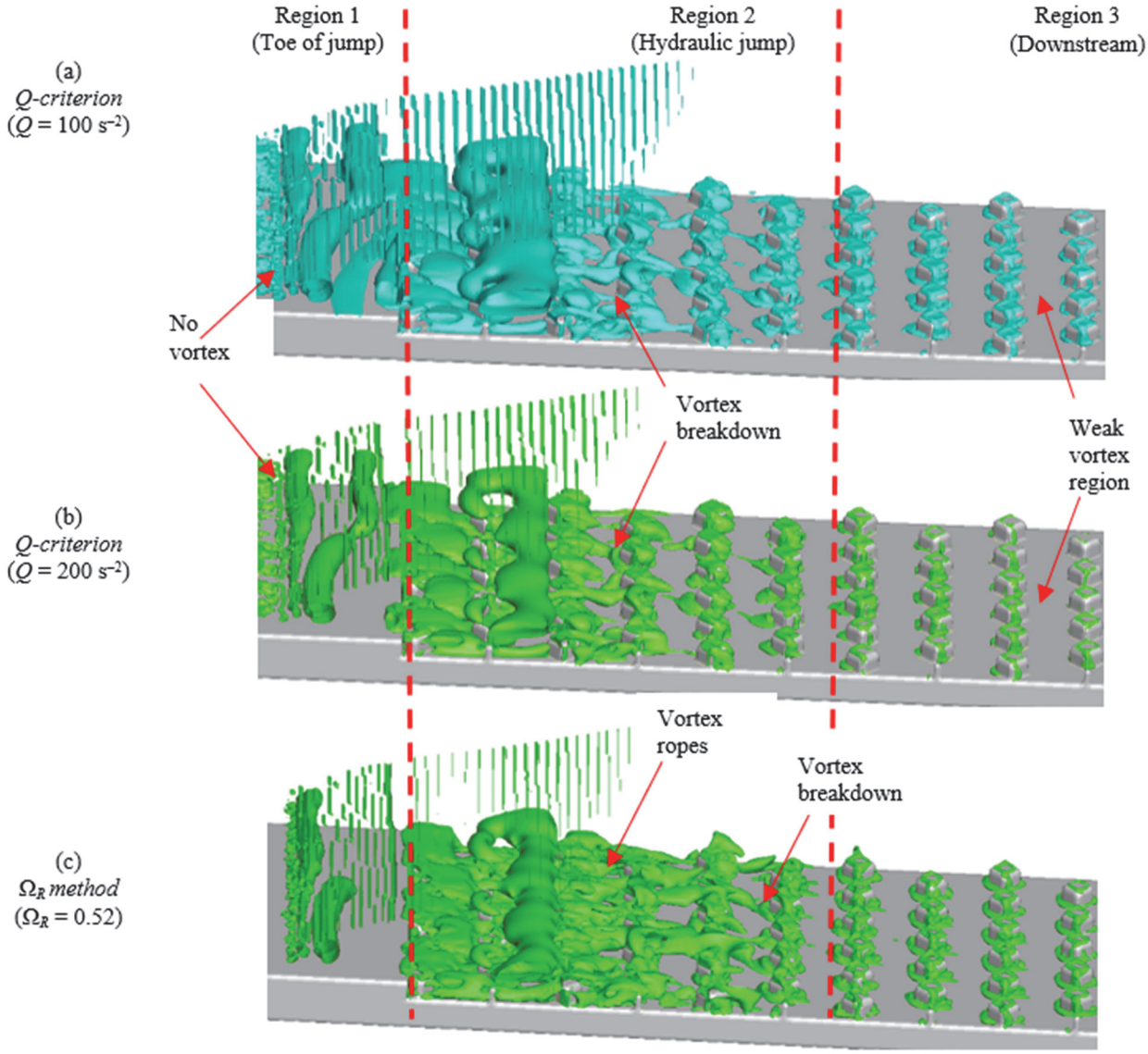


**Figure 4** The vortex structure identification by the Q - criterion (a, b) and $\Omega_R$ method (c) iso-surfaces

Fig. 5 shows the time evolution of the vortex in the hydraulic jump. The vortex formed is associated with a roller-up at the toe of the hydraulic jump [1]. Vortex breaking is usually rapid but has been successfully captured by the $\Omega_R$ method. Over time, the vortex forming, growing, and breaking is reasonably apparent at the jump toe zone. The vortex formed and broken has a characteristic frequency related to the roll-up frequency at the toe jump. This frequency will cause arterial pressure leading to cavitation that can occur in the rough abutment. The bubble entrainment is cyclic.

The rough blocks are arranged with a crest equal to the bottom channel, not directly to conflict with the flow. The flow immediately after the jumper at the second and third rough rows position has strong eddy currents. After these rough bands, the flow energy decreases, the eddy current structure loses its continuity, and the broken eddy is gradually formed. Negative vortices and positive vortices are also observed in this region. In addition, the vortex structure is the primary cause of energy dissipation [19]. The rough bed structure can connect the vortex structure near the wall. Therefore, the vortex exists mainly near the rough block surface as a downstream vortex with sizeable spreading width. The result is that the rough bed has efficient dissipation energy.

Fig. 5 not only shows the vortex structure but also shows the flow velocity distribution in it. As observed, the velocity and lifting height of the vortex structure on the rough bed zone decreased quite rapidly, making the range area of the vortex structure decrease as well. As a result, the fragmentation and influence of the vortex structure are reduced. As observed from Fig. 5, the vortex structure on the rough bottom region continuously acts as a stable "rolling bearing", and it hardly changes shape with time.

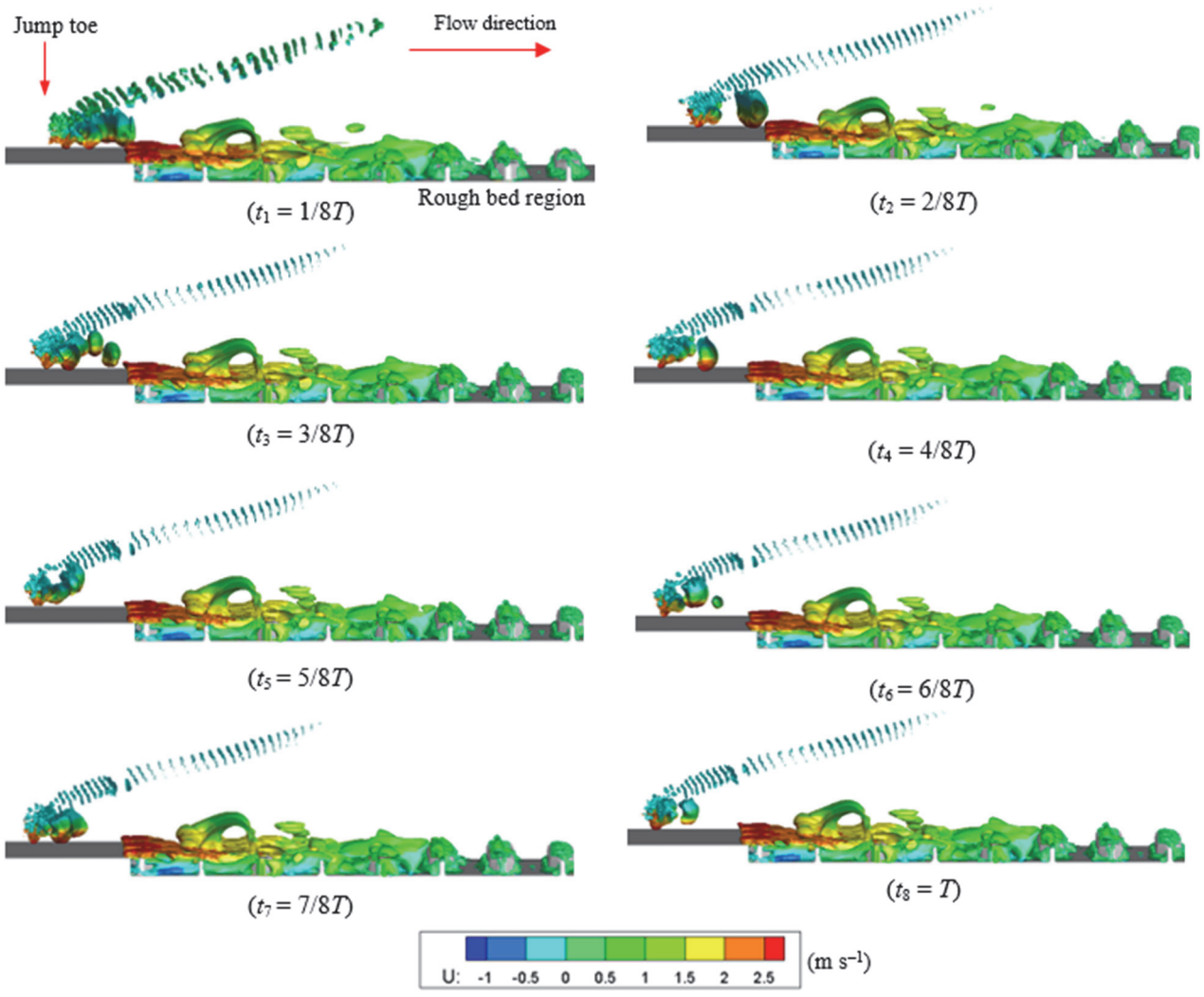


**Figure 5** (Color online) Vortex structure evolution in the hydraulic jump on the rough bed by $\Omega_R$ method

Fig. 6 shows the contours of the instantaneous distribution of Liutex on the three sections from upstream to downstream. A weak vortex zone appeared in section 1 near the toe of the jump, as shown in Fig. 6b. Fig. 6c shows a strong vortex occurring in the roughened bed and above the roughened top region, further demonstrating the strong energy dissipation in this region. The figure also shows the vortex ropes that appeared along the gap between the roughened bed. Fig. 6d shows a significant vortex magnitude and zone decrease after passing rows 2$^{nd}$ and 3$^{rd}$ of the rough block. The weakening of the vortex magnitude indicates causes of the vortex breakdown phenomenon. Therefore, the rough bed dissipates kinetic energy well, resulting in a shorter basin than the smooth bed, which clearly shows the influence of the rough bed on the vortex structure. These results also agree with the experimental

observation of Bejestan and Neisi [3], thus suggesting that the vortex characteristics were well predicted.

To further clarify the local influence of vortex in hydraulic jump, in this study, the vorticities transport equation was employed to analyze flows as follows:

$$\frac{d\omega}{dt} = (\omega\cdot\nabla)V - \omega(\nabla\cdot V) + \frac{1}{Re}(\nabla^2\omega) \tag{9}$$

where $V$ is the velocity, $\omega$ represents the vorticity, and $Re$ is the Reynolds number.

From Eq. (9), we can obtain the vortex production on the mid-plane of the channel ($y$ = 25 cm) as follows [20]:

$$\frac{d\omega_y}{dt} = \left[(\omega\cdot\nabla)V\right]_y - \left[\omega(\nabla\cdot V)\right]_y + \left[\frac{1}{Re}(\nabla^2\omega)\right]_y \tag{10}$$

$$\left[(\omega\cdot\nabla)V\right]_y = \omega_x\frac{\partial V_y}{\partial x} + \omega_y\frac{\partial V_y}{\partial y} + \omega_z\frac{\partial V_y}{\partial z} \tag{11}$$

$$\left[\omega(\nabla\cdot V)\right]_y = \omega_y\left(\frac{\partial V_x}{\partial x} + \frac{\partial V_y}{\partial y} + \frac{\partial V_z}{\partial z}\right) \tag{12}$$

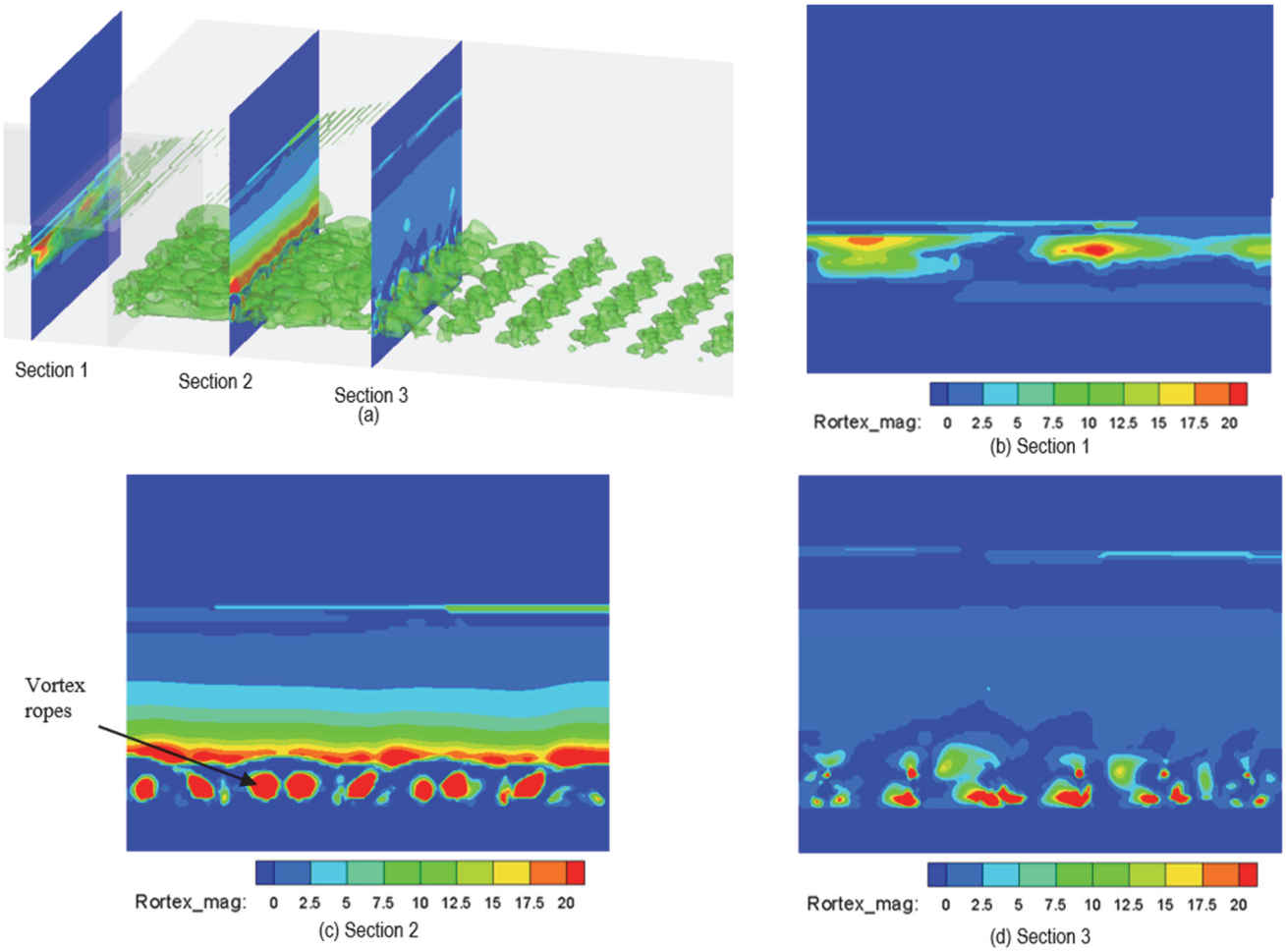


**Figure 6** Contours of instantaneous distribution of Liutex on the three sections

The vorticity production in the turbulence flow is attributed to three parts. The first term, i.e., $(\omega\cdot\nabla)V$, is named the vortex stretching by the swirling and stretching of the flow vorticity. The second term, i.e., $\omega(\nabla\cdot V)$, is the vortex dilatation caused by the fluid compressibility to the vorticity. The third term, i.e., $(1/Re)\cdot(\nabla^2\omega)$, represents the effect of viscous diffusion, and due to the effect being significantly smaller than the other terms can be omitted [20, 21].

Fig. 7 compares the vorticity distribution of the Liutex (Fig. 7a) with vortex stretching (Fig. 7b) and vortex dilatation (Fig. 7c) on the plane $XZ$ at one typical instant. It can be observed from Fig. 7 that the variation of vorticity distribution is strongly associated with the rough bed region and free surface. Fig. 7b indicates that vortex stretching plays a dominant role in the vorticity of the hydraulic jump. Fig. 7c shows the fluctuating characteristics of the free surface focused on the influence of air-water on the hydraulic jump.

From the observation of Fig. 7, the vortex process is associated with the vortex stretching part. It shows that the rough bed has a major role in causing the vortex in the appearance of hydraulic jumps. Figs. 7b and c show that the vorticities are marked by a clockwise rotation (positive vorticity) and an anti-clockwise one (negative vorticity). Fig. 7c shows the vortex dilatation, which causes fluid compressibility to the vorticity. The aeration and free-surface fluctuations occur at the hydraulic jump's roll-up surface. Furthermore, Fig. 7c also shows that there is an enormous vortex (shear) but no rotation (no vortex) at the

boundary layer. As can be observed from Fig. 7a, c the Liutex effectively removes the influence of the boundary layer. The result, the vortex is vorticity without shear, as reported by Liu et al. [9].

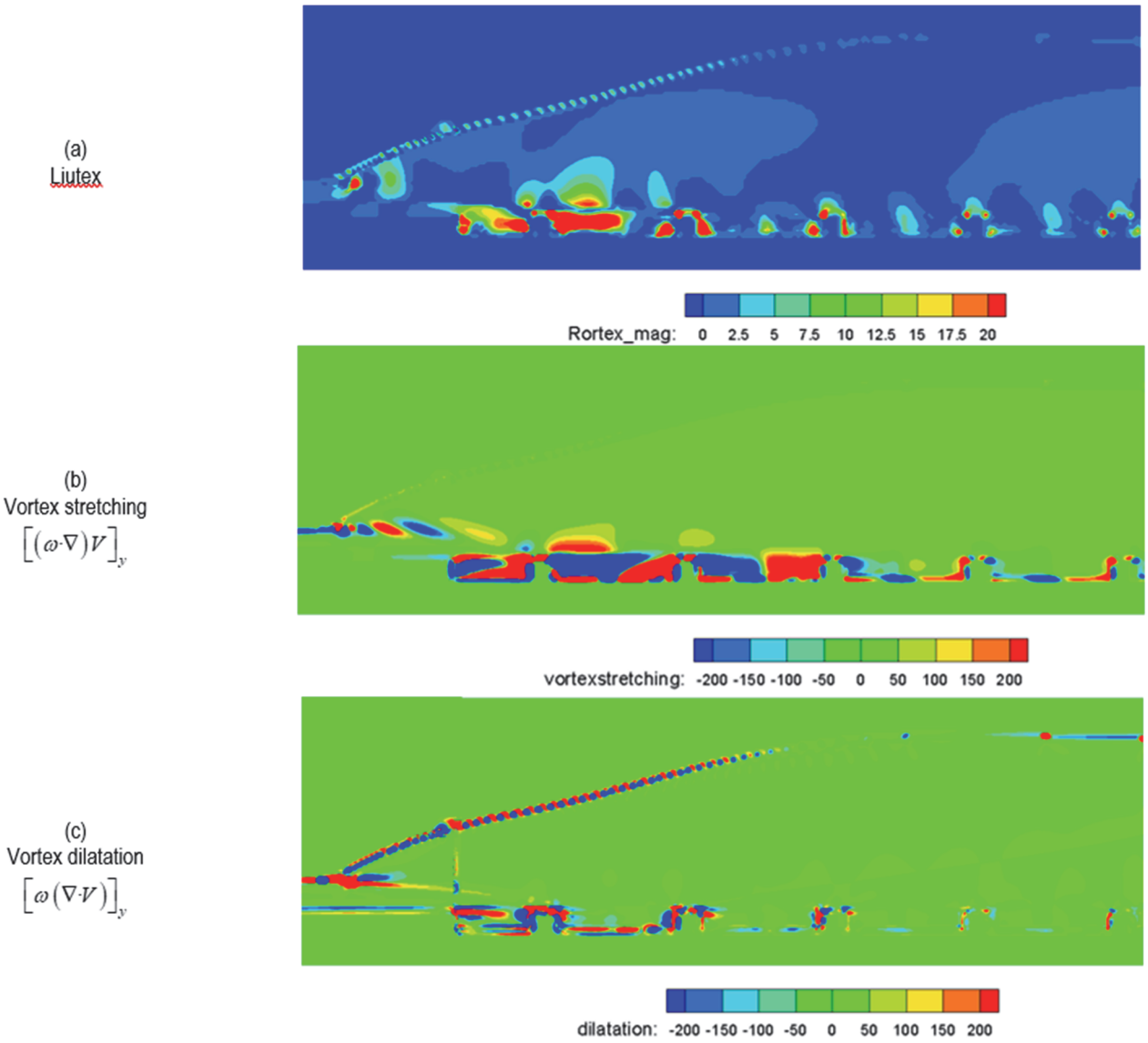


**Figure 7** (Color online) Contour line of Liutex (a), vortex stretching (b), vortex dilation (c), in plane *XZ*

## 4 CONCLUSIONS

The dissipation of energy downstream of hydropower projects is a significant issue. Therefore, the hydraulic jump with rough blocks at the bottom channel is simulated using CFD simulation with the RNG $k$-$\varepsilon$ turbulence model. To investigate the capacity to capture vortex structure in turbulent flows of the rough bed, we used the $Q$-criterion and $\Omega_R$ methods. The analysis has shown that the $\Omega_R$ method has more performance in determining the vortex structure.

The evolution and break of vortex in the hydraulic jump are visualized and analyzed. The vortex structure evolution at the toe of the hydraulic jump has a period in time. At the rough block rows 2$^{nd}$ and 3$^{rd}$, the vortex forms a vortex rope that moves downstream and then breaks. The vortex-shedding region represents a significant energy attenuation of the flow. Therefore, the rough bed dissipates kinetic energy well.

The velocity and lifting height of the vortex structure on the rough bed zone decreased quite rapidly, decreasing the range area of the vortex structure. As a result, the fragmentation and influence of the vortex structure are reduced. The vortex structure on the rough bottom region continuously acts as a stable "rolling bearing", and it hardly changes shape with time. This result helps to better understand the evolution of the vortex and its effect on the hydraulic jump.

### Acknowledgement

The project is supported by the Hanoi University of Civil engineering, Hanoi, Vietnam. This work was completed using the Liutex UTA and Omega-Liutex UTA codes shared by Chaoqun Liu of the University of Texas at Arlington.

## 5 REFERENCES

[1] Viti, N., Valero, D., & Gualtieri, C. (2019). Numerical Simulation of Hydraulic Jumps. Part 2: Recent Results and Future Outlook. *Water*, *11*(1), 28.

https://doi.org/10.3390/w11010028
[2] Peterka, A. J. (1978.) *Hydraulic Design of Stilling Basins and Energy Dissipators.* Department of the Interior, Bureau of Reclamation.
[3] Bejestan, M. S. & Neisi, K. (2009). A new roughened bed hydraulic jump stilling basin. *Asian journal of applied sciences*, *2*(5), 436-445. https://doi.org/10.3923/ajaps.2009.436.445
[4] Tokyay, N. D. (2005). Effect of channel bed corrugations on hydraulic jumps. *Impacts of Global Climate Change*, 1-9. https://doi.org/10.1061/40792(173)408
[5] Nikmehr, S. & Aminpour, Y. (2020). Numerical Simulation of Hydraulic Jump over Rough Beds. *Periodica Polytechnica Civil Engineering*, *64*(2), 396-407. https://doi.org/10.3311/PPci.15292
[6] Hunt, J. C., Wray, A. A., & Moin, P. (1988). Eddies, streams, and convergence zones in turbulent flows. Studying turbulence using numerical simulation databases. 2. *Proceedings of the 1988 summer program*.
[7] Gao, Y. & Liu, C. (2018). Rortex and comparison with eigenvalue-based vortex identification criteria. *Physics of Fluids*, 30(8), 085107. https://doi.org/10.1063/1.5040112
[8] Liu, C., Gao, Y., Tian, S., & Dong, X. (2018). Rortex - A new vortex vector definition and vorticity tensor and vector decompositions. *Physics of Fluids*, *30*(3), 035103. https://doi.org/10.1063/1.5023001
[9] Liu, C. et al. (2019). Third generation of vortex identification methods: Omega and Liutex/Rortex based systems. *Journal of Hydrodynamics*, *31*(2), 205-223. https://doi.org/10.1007/s42241-019-0022-4
[10] Liu, C., Wang, Y., Yang, Y. et al (2016). New omega vortex identification method. *Science China Physics, Mechanics & Astronomy*, (8), 56-64. https://doi.org/10.1007/s11433-016-0022-6
[11] Tran, C. T. & Pham, D. C. (2022). Application of Liutex and Entropy Production to Analyze the Influence of Vortex Rope in the Francis-99 Turbine Draft Tube. *Tehnički vjesnik*, *29*(4), 1177-1183. https://doi.org/10.17559/TV-20210821070801
[12] Dong, X., Gao, Y., & Liu, C. (2019). New normalized Rortex/vortex identification method. *Physics of Fluids*, *31*(1), 011701. https://doi.org/10.1063/1.5066016
[13] Wang, L., Zheng, Z., Cai, W. et al. (2019). Extension Omega and Omega-Liutex methods applied to identify vortex structures in viscoelastic turbulent flow. *Journal of Hydrodynamics*, *31*(5), 911-921. https://doi.org/10.1007/s42241-019-0045-x
[14] Xu, H., Cai, X., & Liu, C. (2019). Liutex (vortex) core definition and automatic identification for turbulence vortex structures. *Journal of Hydrodynamics*, *31*(5), 857-863. https://doi.org/10.1007/s42241-019-0066-5
[15] Tran, C. T. et al. (2020). Prediction of the precessing vortex core in the Francis-99 draft tube under off-design conditions by using Liutex/Rortex method. *Journal of Hydrodynamics*, *32*, 623-628. https://doi.org/10.1007/s42241-020-0031-3
[16] Liu, C. et al. (2019). A Liutex based definition of vortex axis line. *arXiv preprint arXiv*:1904.10094. https://doi.org/10.48550/arXiv.1904.10094
[17] Samadi-Boroujeni, H. et al. (2013). Effect of triangular corrugated beds on the hydraulic jump characteristics. *Canadian Journal of Civil Engineering*, *40*(9), 841-847. https://doi.org/10.1139/cjce-2012-0019
[18] Ghaderi, A. et al. (2020). Characteristics of free and submerged hydraulic jumps over different macroroughnesses. *Journal of Hydroinformatics*, 22(6), 1554-1572. https://doi.org/10.2166/hydro.2020.298
[19] Wu, Z. et al. (2021). Analysis of the influence of transverse groove structure on the flow of a flat-plate surface based on Liutex parameters. *Engineering Applications of Computational Fluid Mechanics*, *15*(1), 1282-1297. https://doi.org/10.1080/19942060.2021.1968955
[20] Ji, B., et al. (2014). Numerical simulation of three-dimensional cavitation shedding dynamics with special emphasis on cavitation - vortex interaction. *Ocean Engineering*, 87, 64-77. https://doi.org/10.1016/j.oceaneng.2014.05.005
[21] Tran, C., Bin, J., & Long, X. (2019). Simulation and Analysis of Cavitating Flow in the Draft Tube of the Francis Turbine with Splitter Blades at Off-Design Condition. *Tehnicki vjesnik - Technical Gazette*, *26*(6). https://doi.org/10.17559/TV-20190316042929

**Contact information:**

**Cong Trieu TRAN**
(Corresponding Author)
Hanoi University of Civil Engineering,
55 Giai Phong, Hanoi, Vietnam
E-mail: trieutc@huce.edu.vn

**Cong Ty TRINH**
Hanoi University of Civil Engineering,
55 Giai Phong, Hanoi, Vietnam
College of Water Resource & Hydropower,
Sichuan University,
Chengdu 610065, China
Email: tytc@huce.edu.vn